UNIVERSITÀ DEGLI STUDI DI PADOVA

Dipartimento di Fisica e Astronomia "Galileo Galilei"

Corso di Laurea in Fisica

Tesi di Laurea

Lifetime measurements with fast-timing scintillators

Relatore

Prof. Daniele Mengoni

Correlatore

Dr. Andrés Illana Sisón

Dr. Alain Goasduff

Laureanda

Marta Magalini

Anno Accademico 2018/2019

Contents

Chapter 1

Introduction

Lifetime of a nuclear excited state is one of the main observables in the nuclear structure studies. The lifetime determines the reduced electromagnetic transition probability which is used to be compared with predictions derived by using theoretical nuclear structure models and thus provides an essential nuclear observable to test the model dependent structure of the nuclear excited states.

There are different ways to measure lifetime τ of an excited state and their use depends on the magnitude of the value we are interested in. Usually, the techniques for τ measurements are divided into direct methods, such for example tagged spectroscopy, pulsed beam technique, γ-γ coincidence, that cover the time range from *ns* to minutes, and indirect methods, generally based on the Doppler effect, such as the Recoil Distance Doppler Shift or the Fraction Doppler Shift, which allow to measure lifetime down to tens of *fs*. In this research we focused on the γ-γ coincidence technique and its implementation with the scintillation detectors, especially the inorganic $LaBr_3(Ce)$ scintillators.

Nowadays, the Cerium doped Lanthanum bromide material is one of the fastest scintillators commercially available. It has a range of excellent properties, such as the best energy resolution among all scintillators, sub-nanosecond time resolution, almost perfect light yield proportionality and good stability of the emitted light with temperature. Since it combines good energy resolution and fast response, it owns a great potential for applications such as gamma-ray spectroscopy, medical imaging and lifetime measurements. Moreover, this kind of scintillators provides high intrinsic gamma-ray detection efficiency and a photon yield of 63 photons/keV. In the γ-γ coincidence technique, the fast coincidences between the radiation populating and de-exciting a nuclear level allows the measurements of this nuclear level lifetimes down to a few picoseconds. The sensitivity in lifetime measurements with scintillators is directly determined by the time resolution of detectors in use and therefore its size, shape and doping. The optimization of the electronic circuit and the detector operation parameters is also needed to achieve the best performance of the set-up.

In the first part of this work, the main characteristics and components of a scintillator detector, together with the main pick-off methods in timing measurements, are discussed. In the second part, timing performance and some important linked properties of seven $LaBr_3(Ce)$ scintillators of two different kind, equipped with a 3"x3" cylindrical crystal and a 1.5"x1.5"x1" truncated cone crystal respectively, are analyzed. Energy resolution, efficiency and time resolution have been evaluated by using different radioactive type of sources and the detector time response has been optimized by the tuning of the electronics parameters, especially the constant fraction discriminator parameters. Finally, the lifetime of the 121keV-energy state of ^{152}Sm has been measured thanks to the slope method. Assuming no background distribution, the experimentally obtained "delayed" time distribution is a convolution of the normalized prompt response function (PRF) of the set-up with an exponential decay. The slope method is used for lifetime which are larger than the FWHM of the PRF and the lifetime is obtain by a simple fit of the exponential tail of the distribution. The experiment was performed at the Legnaro National Laboratory as part of the GALILEO project.

Chapter 2

Scintillation detectors

In this chapter the main features and components of a scintillation detector will be presented with attention to the peculiar properties of a LaBr(Ce) crystal and all those aspects that influence the timing measurements.

2.1 Scintillation Detector Principles and Materials: LaBr(Ce)

A scintillation detector is a device that permits the detection of ionizing radiations such as for example γ rays, both by exploiting the scintillation light produced by certain materials when they interact with these radiations and by converting it in an electrical pulse, thanks to photomultiplier (PMT) tubes.

The ideal scintillation material should convert the kinetic energy of ionizing particle into detectable light with a high efficiency and this conversion should be linear, which means that the light yield should be proportional to the deposited energy, in order to preserve the initial energy information. The *medium* should be transparent to the wavelength of its own emission so that the light collection could be good; and the decay time of the induced luminescence should be short enough to generate fast signal pulses and preserve time information. The scintillators are divided in organic scintillators, which tend to have the best light output and linearity but are relatively slow in their response time, and inorganic scintillators, whose high Z-value of the constituents and high density favour their choice in gamma-ray spectroscopy.

The scintillation mechanism in inorganic materials depends on the energy states, determined by the crystal lattice of the material. The electrons, typically collocate in the valence band, have available only discrete bands of energy, as shown in Figure 2.1. When energy is absorbed by the material an electron can be elevated from its normal position in the valence band across the gap into the conduction band, where it is free to move throughout the crystal, leaving a hole in the valence band. In the pure crystal, the return of the electron to the valence band with the emission of a photon is an inefficient process, because of the self-absorption. To increase the probability of visible photon emission, small amounts of an impurity, called activators, are commonly added to inorganic scintillators. These impurities create special sites in the lattice and the normal energy band structure is modified from that of the pure crystal. As a result, there will be energy states created in the forbidden gap through which the electron can de-exited back to the valence band, and finally the crystal has become transparent to the scintillation light.

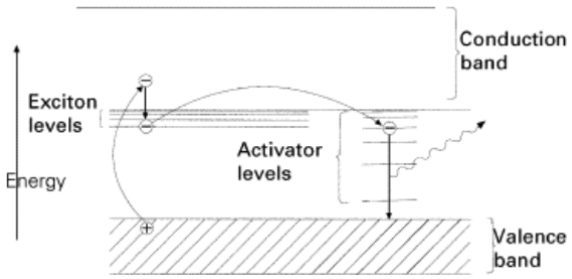

Figure 2.1: Energy band structure of an activated crystalline scintillator [1].

In our experiment we use $LaBr_3$(Ce) crystals that present outstanding scintillator characteristics, including high effective Z and density, fast decay times, emission wavelength well matched to the common photocathodes, excellent energy resolution and high photon yield (63 photons/keV) [1]. Compared with other options, $LaBr_3$(Ce) has a good energy resolution (Figure 2.2) and its fast decay time is also a big advantage over slower inorganic scintillators for applications involving high counting rates or fast timing.

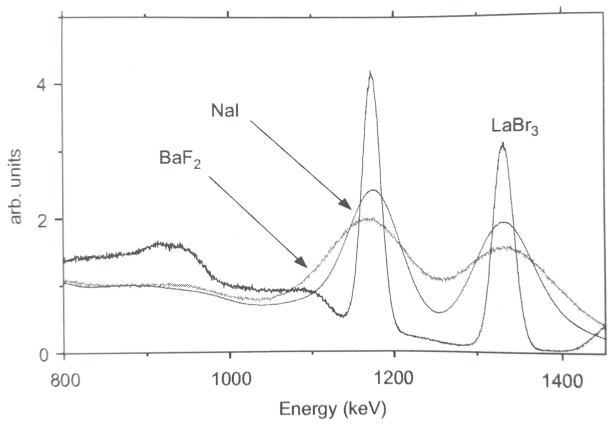

Figure 2.2: Comparison of the ^{60}Co pulse height spectrum measured with 1-inchx1-inch $LaBr_3$, NaI and BaF_3 [1].

Generally, there are two primary drawbacks associated to these scintillators. First, the intrinsic radioactivity from ^{138}La results in the intrinsic background of about 1-2 $counts/cm^2s$. Second, an anisotropic thermal expansion causes internal stresses as crystal cool after growth due to the hexagonal crystal structure of these crystals; and careful procedures are required to prevent cracking of large crystals. Finally, the lanthanum halides have also been shown to have other favourable characteristics, for example they have relatively constant light yield and energy resolution over a wide range of temperatures.

One of the key aspects in this kind of detector is the collection of light that is emitted isotropically from the track of the ionizing particle. As a matter of fact, the light collection conditions affect the energy resolution of a scintillator in two different ways: at first, the statistical broadening of the response function will gradually worsen as the number of scintillation photons, that contribute to the measured pulse, reduces; and at second, the uniformity of the light collection will determinate the variation in signal pulse amplitude, as the position of the radiation interaction is varied throughout the scintillator. Both of these factors will directly influence the choice of the pick-up method, as shown in Chapter 3.

Since the scintillation light is emitted in all directions, only a limited fraction can travel directly to the surface at which the PM tube is located. In order to collect the remaining part of light, this must be reflected at least once to the scintillator surfaces; and for this reason, the scintillator is usually surrounded by a reflecting material except the surface which the PM tube is applied to. Better light collection efficiency is achieved by using a guide pipe, to physically couple the scintillator to the PM tube and to operate as a guide for the scintillation light.

2.2 Photomultiplier Tube and Photodiodes

Since the scintillation light emitted in the crystal is extremely weak, a device that converts this pulse into a corresponding electrical signal is necessary. The photomultiplier tube accomplishes this task, converting light signals that typically consist of a few hundred photons into a current pulse, without adding a large amount of random noise to the signal. The simplified structure of a typical PM tube is shown in Figure 2.3.

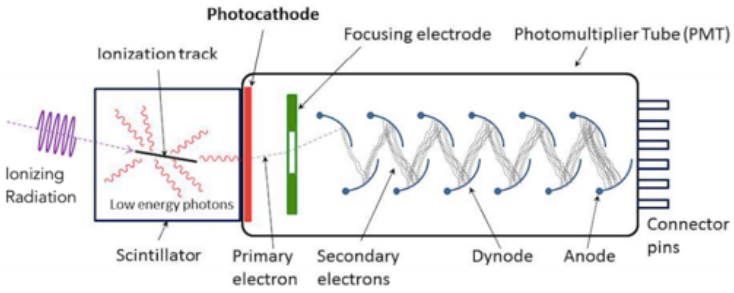

Figure 2.3: Basic scheme of a PM tube.

Inside the tube, vacuum conditions are achieved so that low-energy electrons can be accelerated efficiently by internal electric fields. The two major components inside the tube are a photosensitive layer, the photocathode, coupled with an electron multiplier structure. The photocathode is used to convert as many of the incident light photons as possible into low-energy electrons. These photoelectrons give rise to a pulse of similar time duration of the one of scintillation light. The electron multiplier section, composed by a series of dynodes at growing potential, provides an excellent collection geometry for the photoelectrons, as well as serving as an amplifier to greatly increase their numbers. After amplification, a typical scintillation pulse will give rise to 10^7-10^{10} electrons, a sufficient amount to serve as the charge signal for the original scintillation event. This charge in finally collected at the anode.

Most PM perform this charge amplification in a very linear way, producing an output pulse at the anode that remains proportional to the number of original photoelectrons over a wide range of amplitude; as to preserve the information about the initial γ ray energy. Furthermore, much of the timing information of the original light pulse is also retained, and this is crucial in our timing coincidence measurements.

Since the time required both for the photoemission in the photocathode and the secondary emission from dynodes is very short (0.1 ns or less), the time characteristics of the PM tube are determined exclusively by electron trajectories. The electron transit time of a PM tube is defined as the average time difference between the arrival of a photon at the photocathode and the collection of the electron pulse at the anode. However, this transit time, that is about 20-80 ns, doesn't cover a primary importance role because it introduces only a fixed delay in the derived signal as it is most likely considered constant. The spread in transit time is a more important quantity instead, because it determines the time width of the pulse of electrons arriving to the anode of the tube.

The timing response of a typical PM tube is illustrated in figure 2.4.

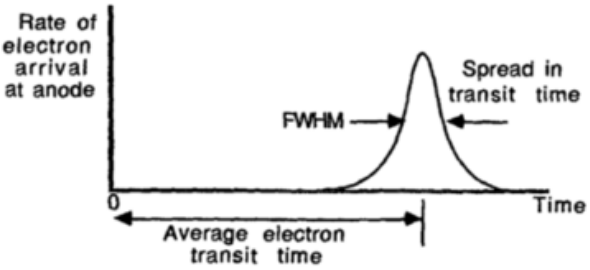

Figure 2.4: Response of a PM tube to a short pulse of light on the photocathode [1].

The critical area in determining the timing proprieties inside the PM tube is the distance between the photocathode and the first dynode. To allow the uniform collection over large photocathodes, this gap is kept fairly large compared to the interdynode distances (Figure 2.5). The difference in path between a photoelectron leaving the center of the photocathode and one which located at the edge, is often a dominant factor in the observed spread in transit time. For this reason, the shape of the majority of the photocathode is curved, to minimize the transit time spread across its diameter. A second source of transit time spread arises from the distribution in initial velocities of photoelectrons leaving the photocathode. This effect can be minimized by using large voltage difference between the photocathode and the first dynode.

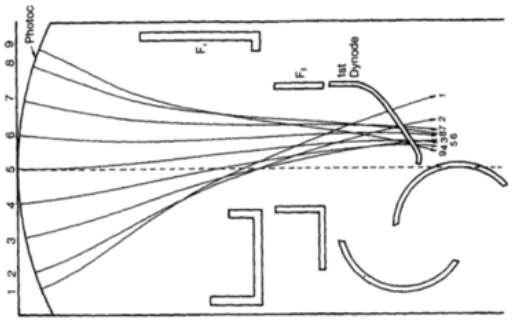

Figure 2.5: Examples of trajectories of electrons accelerated from the photocathode to the first dynode in a PM tube [1].

The observed spread range of transit time also depends on the number of initial photoelectrons per pulse. If the distribution in the various possible transit time is assumed to be Gaussian, so then the statistical theory predicts that the relative spread in transit times should vary inversely with the square root of the number of photoelectrons. Thus, high light yield from a scintillator is important in timing applications, as well as in pulse height measurements, so that the choice of the LaBr(Ce) crystal, which have one of the most high yield, is consistent. The time spread attributable to the multiplier section also decreases with the increasing of the interdynode voltage; and the best timing performance is normally obtained by operating with the tube at the maximum voltage possible.

Chapter 3

Timing measurements in nuclear physics

In this chapter the main pick-up methods and their associated errors in timing measurements will be discussed, as well as the principal characteristics of a time spectrum.

The accuracy by which timing can be measured depends both on the proprieties of the specific detector (as discussed in Chapter 2) and the type of electronics used to process the signal. The best timing performance is obtained by the fastest detectors, namely, those in which the signal is collected most rapidly; and this will be clearly evident when the time resolution of the two type of detector of our experiment will be analyzed.

The most fundamental operation in timing measurements is the generation of a logic pulse, whose leading edge indicates the time of occurrence of an input linear pulse; this will allow to construct a time spectrum. Electronic devices that carry out this function are called *pick-off units* or *triggers*. In timing measurements there are two main pick-off methods that will be discussed in detail: Leading Edge and Constant Fraction Discriminator.

It must be considered that some factors could inevitably cause some degree of uncertainty in deriving the timing signal. Sources of inaccuracy are conventionally divided into two main categories: those that apply when the input pulse amplitude is constant, usually called sources of time jitter, whereas those effect that derive primarily from the variable amplitudes of input pulses, named amplitude walk. Relative importance of these two categories depends on the dynamic range expected in the input pulse amplitude. The best timing performance will be achieved if the input pulses are confined to a very narrow range in amplitude, because the time jitter will be the only uncertain source. An important source of time jitter is the random fluctuations in the signal pulse size and shape. These fluctuations can be attributed to several causes, such as the electronic noise added by components that process the linear pulse prior to the time pick-off or the discrete nature of the electronic signal generated in the detector.

3.1 Timing algorithms: Leading Edge

The easiest and most direct method to carry out the time pick-off is to fix a discrimination level and register the time when the pulse crosses this level. This timing method is called Leading Edge, and it is usually adopted when the dynamic range of the input pulses is not large.
The effect of time jitter on leading edge is shown in figure 3.1. The random fluctuations superimposed on signal pulses of an identical size and shape may generate an output logic pulse at somewhat different times respect to the centroid of the pulse. The timing errors will be approximately symmetrical and will increase if the slope of leading edge of the pulses is decreased.

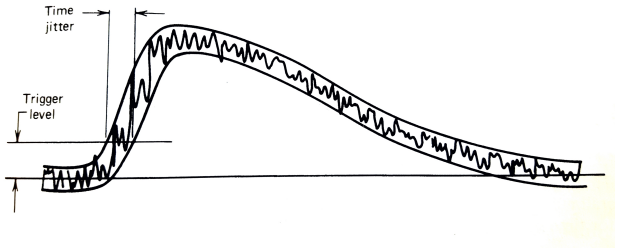

Figure 3.1: The time jitter in leading edge triggering [1].

Concerning the amplitude walk instead, associated with a Leading Edge trigger, it is graphically demonstrated in figure 3.2. The two shown pulses have identical true time of origin but they give rise to out-put logic pulses that differ substantially in their timing.

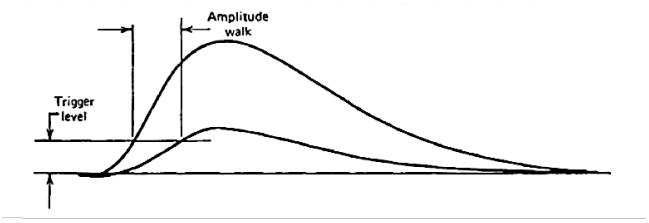

Figure 3.2: Amplitude walk in leading edge triggering [1].

Even if the amplitude is constant, walk can still take place if changes occur in the shape of the pulse. Detectors with variable charge collection time, such as germanium detectors, produce output pulses with a variable rise time as in figure 3.3. All changes that occur in the pulse shape before the discrimination point will affect the timing and can constitute another source of uncertainty timing, called time walk. The sensitivity of leading edge triggering is not dramatically affected by time walk since the amplitude and shape variation is minimized by setting the discrimination level as low as possible; but the discrimination point should be in a region of steep slope to also minimize uncertainties due to the jitter. A practical compromise is given by setting the threshold around 10-20% of the average pulse amplitude.

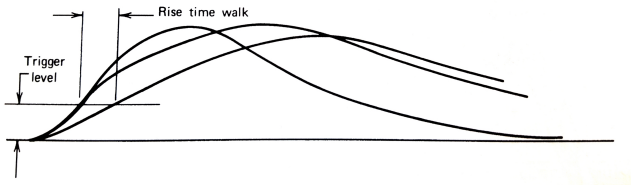

Figure 3.3: Time walk in leading edge triggering [1].

3.2 Timing algorithms: Constant Fraction Discriminator

When the Leading Edge triggering is applied to pulses with a wide amplitude range, amplitude walk often results in large timing uncertainties. Furthermore, it is empirically discover that the best leading edge timing characteristics are obtained when the timing discriminator is set around 10-20% of the pulse amplitude. These observations led to the development of a new time pick-off method, that produces an output signal just at a fixed time after the leading edge of the pulse has reached a constant fraction of the peak pulse amplitude. For all the pulses with a constant shape, although the pulse amplitudes differ widely, the time at which the waveform crosses the x-axis is independent

with respect of the amplitude, and depends on the shaping time constant chosen for the network only. Compared to the LE timing, crossover methods greatly reduce amplitude walk and also keep the jitter low. The electronic shaping steps required to carry out constant fraction timing are shown in figure 3.4.

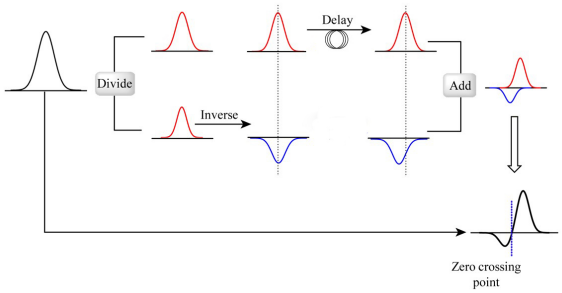

Figure 3.4: Constant Fraction Discriminator method.

The process involves taking the PM output and divide the signal into two parts: one is multiplied by the fraction that correspond to the desired timing fraction of full amplitude and then is inverted, the other part is delayed for a bigger amount of time than the pulse rise time. At the end of these processes the resultant waveforms are summed together. The time that this pulse crosses the zero axis is independent in relation to the pulse amplitude, and corresponds to the time at which the pulse reaches the fraction of its final amplitude.

In general, Leading Edge triggering gives the best timing resolution mainly for those signal pulses whose amplitudes are restricted to a narrow range and whose shape do not vary. When pulses with a wide range of amplitude are processed, leading edge methods show large amplitude walk. Constant fraction timing methods are very effective in reducing amplitude walk when the pulse shape does not change. In our experimental case, scintillation detectors produce pulses of fixed shape when a given type of radiation is involved; for this reason we selected the CFD pick-up method in our measurements. The procedure used to determinate the zero-cross of the waveform by the digitizer it will be described in Chapter 4.

3.3 Time spectrum

Two independent detectors are considered, irradiated by a common radioisotope source that is assumed to emit at least two detectable quanta in true coincidence; that means both of the radiations arise from the same nuclear event within the source. These quanta will be considered as the "start" and "stop" signals elaborated inside the digitizer. The distribution of time intervals between start and stop pulses is called time spectrum (figure 3.5). The abscissa shows the time interval length (or channel number), while in the ordinate the counts per channel are reported. The full width at half maximum of the time distribution is often used as a measure of the overall timing uncertainty in the measurement system, this is called the time resolution.

We furthermore assume that for all the true coincidences, the nuclear decay scheme is such that there is not an appreciable time delay between the emission of both radiations, or, in other words, the mean lifetime of the excited states involved is smaller than the statistical time resolving power of the set-up (about 1ps for fast scintillators). This is the case, for example, of the two double decay of a ^{60}Co source with the emission of two γ at the energy of 1.33 MeV and 1.17 MeV. The time spectrum taken under these conditions will show a peak called *prompt coincidence peak*, whose distribution is approximately Gaussian.

When detectors, timing electronics, and triggering conditions are nearly identical in both branches, then all sources of time jitter and walk should be symmetric. Under these conditions the prompt co-

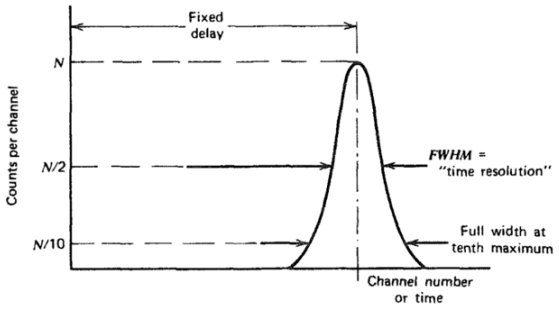

Figure 3.5: Example of a multichannel time spectrum.

incidence peak should also be symmetric with a width that indicates the total contribution of all sources of time uncertainty. In addition to the coincidence events, each detector will typically produce a number of pulses that correspond to the detection of one quanta, for which there may not be a corresponding coincident emission, or for which the coincident radiation escapes detection in the opposite detector. These events are called *chance interval* and their distribution is approximately uniform over the entire time range. In order to improve the ratio of the prompt peak to the chance continuum energy, selection criteria may be used by discarding any events that does not correspond to true coincidences. Figure 3.6 shows an example of the γ-γ coincidences recorded with a ^{60}Co source with no energy selection. As a consequence, it is important that the scintillation detectors have not only an optimum time resolution but also a good energy resolution. Another method to improve the selection of true events is the single-channel method, which means setting a time window to accept only those sequences in which the interval between the start and stop pulses lies within a narrow band. For time spectroscopy, the coincidence unit selects from all the intervals only those in which the time difference between inputs is less than a circuit parameter, known as the *resolving time*. The coincidence resolving time is chosen to be larger than the system time resolution, so that the acceptance time window can fully encompass all true coincidences.

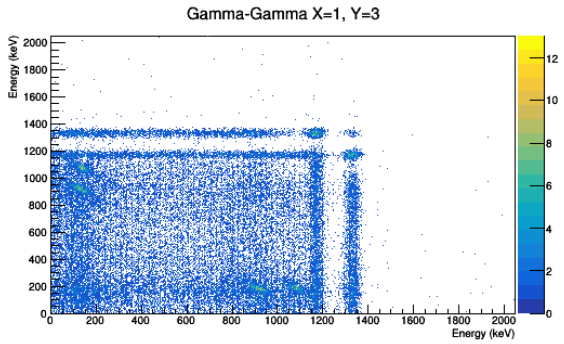

Figure 3.6: Example of a $\gamma - \gamma$ coincidence of a ^{60}Co source with the emission of two photons at the energy of 1.33 MeV and 1.17 MeV.

There are many occasions in which radiations are emitted in the same nuclear decay but are separated in time, because of an intermediate nuclear state of finite lifetime. If this lifetime is bigger than statistical time resolving power of the set-up, and assuming that no time-correlated background contributes to the time distribution, the delayed time distribution in general corresponds to a convolution of the energy-depended prompt time distribution with an exponential decay. This time distribution should then show an exponential tail to the right of the prompt peak. By measuring the time constant of this tail, the decay constant of the intermediate state can be deduced. Acting so, the lifetime of an excited state of ^{152}Sm will be measured, see Chapter 5 for more details.

Chapter 4

Experimental setup

In this chapter the experimental setup of the experiment is briefly presented.

The experimental set-up for this work consisted of 4 $LaBr_3$(Ce) scintillation detectors with a truncated cone shape crystal, with nominal height of 1.5" (38.1 mm) and bases of 1.5" and 1" (35.1 mm), and 3 $LaBr_3$(Ce) scintillation detectors with a cylindrical 3"x 3" crystals (figure 4.1, 4.2). The first kind of crystals were optically connected to Hamamatsu R6233-100SEL Photomultiplier tubes (PMT) [2], while the second to a Hamamatsu R9779 PMTs [3], which have been shown to deliver a nearly linear energy response, i.e. the pulse height vs energy relation. The deviation from linearity is smaller than 2% for pulses with amplitude smaller than 3V.

The scintillators were placed inside the GALILEO support at Legnaro National Laboratory (LNL), with a target-to-detector distance about 10 cm. Each scintillator anode has been connected independently to a CAEN V1730B [4], which is a Flash ADC Waveform Digitizer with 16 channels 14-bit 500 MS/s, that can take a sample every 2 ns for 16 channels at the same time. The parameters for configuration, such as trigger channel, CFD delay, CFD fraction, gates of integration etc. have been manually set using the software interface Kmax [5]. The CFD inside the digitizer allows to increase timing resolution beyond the granularity given by the sampling period of the ADC by interpolating two or more sample points adjacent to the zero crossing. It is possible to select the number of points for this linear interpolation, this parameter will be indicated as CFD interpolation [6].

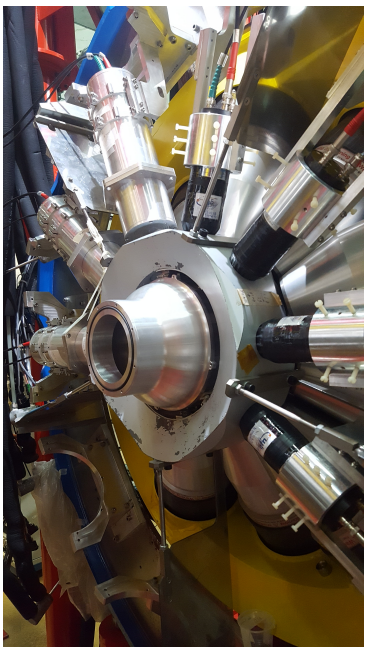

Figure 4.1: The $LaBr_3$(Ce) detectors installed inside the GALILEO support.

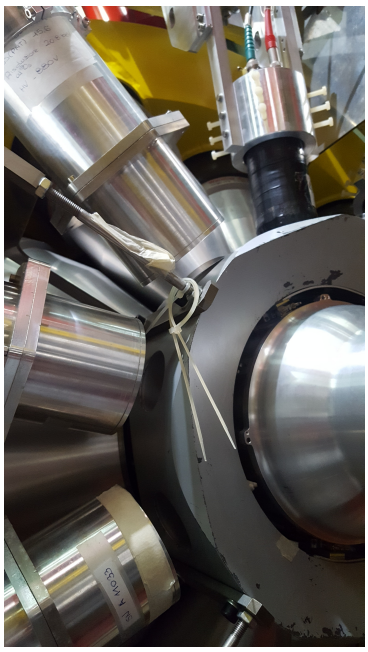

Figure 4.2: The three cylindrical scintillators and one with the truncated cone crystal.

The PMT voltages for all $LaBr_3(Ce)$ detectors have been set initially to 1200V. We used sources of ^{241}Am, ^{137}Cs, ^{60}Co for energy spectra calibration and energy resolution evaluation, this analysis was done also at 1100V. A source of ^{152}Eu was used for the efficiency evaluation of the two type of scintillator. On the other hand, time spectra were obtained by using the $\gamma - \gamma$ coincidence of a ^{60}Co source and time resolution has been optimized by the fine tuning of the constant fraction discriminator parameters (see section 5.1). Once we got the best parameters for time resolution, we finally took measurements again with a ^{152}Eu source, but we chose to use only small scintillators because of their best time performance. Table 4.1 and 4.2 show the activity of each γ source used and the final set of parameters for Sm lifetime measurement respectively.

Table 4.1: Activity of each source and date of its measurement.

Source	Activity (kBq)	Date of measurement
^{241}Am	390	1/06/2015
^{137}Cs	388	1/08/2010
^{60}Co	442	1/08/2010
^{152}Eu	396	1/08/2010

Table 4.2: Voltage and CFD parameters for the ^{152}Sm lifetime measurement. CFD fraction and delay are the typical parameters of this pick-off method, whereas CFD interpolation is the number of point before and after the zero cross of the pulse used by the digitizer for the linear interpolation.

Voltage	CFD fraction	CFD Delay	CFD interpolation
1100 V	50%	2 ns	1

Data taken from each event in a detector are digitized and stored in real time in a large digital memory thank to a data acquisition methodology named *list mode*. These data include information on the energy of pulses from multiple detectors, together with the output of a continuously-running clock, that is sampled at the time of occurrence of each separate pulse. Thus, all events recorded from each detector carry a time stamp. During the measurements, all the data are simply accumulated in the memory, and the analysis is carried out offline after the measurement is completed. This analysis can examine the time stamp information to sense coincident events in separated detectors. This technique allows countering the effect of time walk and time jitter, since both energy and timing information are available for each event and thus timing corrections can be applied.

Chapter 5

Data analysis

In this chapter the main characteristics of the scintillation detectors used in the experiment will be discussed, specifically their energy resolution, photopeak efficiency and performance in timing measurements. Finally the measure of the lifetime of the state at 121 keV of ^{152}Sm will be presented.

5.1 Detector characterization

5.1.1 Energy

The DPP-PHA (Pulse Height Analysis) implemented in the digitizer CAEN V1730B allows the energy evaluation of the signal coming directly from the photomultiplier by means of a Trapezoidal Filter. This filter can be briefly described as a filter which has the capability to transform a signal generated by a PM into a trapezoid which present a flat top whose height is proportional to the amplitude of input pules (for more details see Ref. [6]). The energy information of each event is collected and thus the differential pulse height distribution or energy spectrum can be reconstructed offline using ROOT interface.

The energy resolution R of a detector is conventionally defined as the FWHM of the γ-ray full energy peak in the energy spectrum divided by the location of the peak centroid. This is an important factor to be considered in lifetime measurements, since it enables a proper selection of decay branches and it contributes as well to minimize the time correction. The finite energy resolution of any detector may contain contributions resulting from the separate effects of the charge collection statistic, electronic noise, variations in the detector response over its active volume. For the scintillation detectors, the enhance light collection, the size of the crystals and the fluctuation in PM tube gain from event to event can also influence on the energy resolution.

In our case, the statistical broadening of the peak predominates over other potential sources of resolution loss, and the variation of the resolution with gamma ray energy may be predicted simply by noting that the FWHM of the peak is proportional to the square root of the gamma ray energy; instead the average pulse height produced is directly proportional to the gamma ray energy [1]. Therefore, from the definition of energy resolution:

$$R \equiv \frac{\mathrm{FWHM(keV)}}{E} = \frac{\mathrm{K}}{\sqrt{E}} \tag{5.1}$$

To determinate the energy resolution of the $LaBr_3(Ce)$ detectors and make a comparison at different voltage, gamma rays emitted from a source of ^{241}Am, ^{137}Cs, ^{60}Co were measured with a PM voltage set at 1200V and than at 1100V. For each voltage, second-order polynomial was used to calibrate the digitizer channels of observed peaks to the known gamma-ray energies emitted by the source. Data from all detectors of each type were summed separately and an example of the resultant summed spectra is shown in figure 5.1.

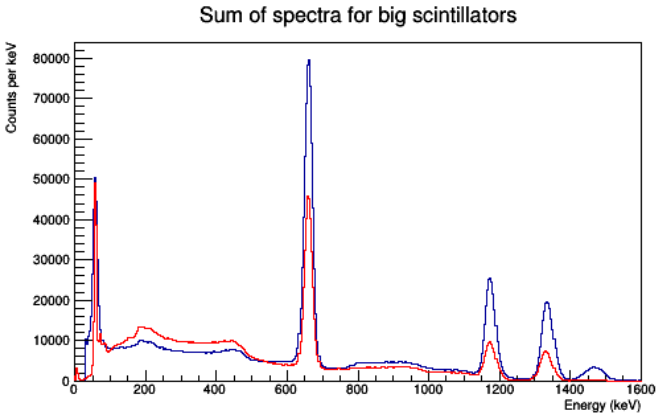

Figure 5.1: Spectra of a source of ^{241}Am, ^{137}Cs, ^{60}Co with a PM voltage of 1200V. The red spectrum comes from the truncated cone shape scintillators instead the blue spectrum is generated by the cylindrical scintillators.

We notice that the cylindrical scintillators, even if they are numerically less, capture in the same time of measure more events than truncated cone ones; as the matter of fact the peaks of their summed spectrum results higher (blue spectrum in figure 5.1). However, this is not true for the first peak ^{241}Am because of the presence of a thin layer of Cu on the first channel that obstructs the γ rays at low energy.

Calculating the standard deviation σ of each peak using a gaussian interpolation on the full energy peak we than obtain the FWHM as FWHM$= 2\sigma\sqrt{2ln(2)}$ and the resolution R by definition. Figure 5.2 shows the various resolutions of the two kind of scintillators at the two voltage, each curve follows the trend of equation 5.2. Table 5.1 reports the value of energy resolution for gamma rays from ^{137}Cs (661.657 keV), conventionally used as a standard for comparison.

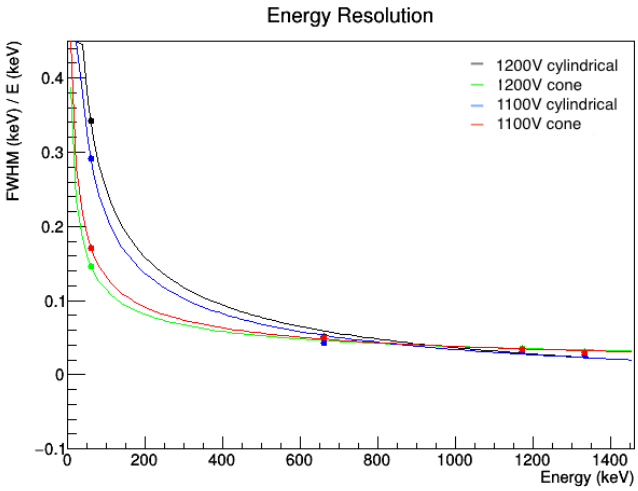

Figure 5.2: Energy resolution of the big cylindrical detectors, called cylindrical, and the small truncated cone detectors, called cone, calculated from the ratio between the full with half maximum and the energy of peaks of a ^{241}Am, ^{137}Cs, ^{60}Co with a PM voltage of 1200V and 1100V.

Table 5.1: Energy resolution of gamma ray of ^{137}Cs (661.657 keV) source at different voltage for the two kind of scintillators

Geometry	FWHM (keV) 1200V	Er(%) 1200V	FWHM (keV) 1100V	Er (%) 1100V
Cylinder	31.83±0.05	4.8	28.24±0.04	4.3
Truncated cone	30.84±0.05	4.7	33.18±0.05	5.0

We observe that the most significant difference between energy resolution is at low energy (^{241}Am 119 keV γ-ray) where the cylindrical scintillators have a resolution nearly double respect to the trun-

cated cone scintillators which maybe be expected as a result of their larger volume. At higher energy the difference becomes smaller and also the value of voltage does not influence in a relevant way the resolution.

5.1.2 Efficiency

A high gamma-ray detection efficiency is a required feature in $LaBr_3(Ce)$ detectors. We evaluated the *absolute full energy peak* efficiency of both kind of scintillators with a ^{152}Eu source. The PMT voltage was set to 1200V and the CFD fraction, interpolation and delay to 25%, 1, 1ns for truncated shape scintillator and 75%, 1, 5ns for the cylindrical ones. *Absolute* efficiency is defined as in 5.2 :

$$\epsilon_{abs} = \frac{number\ of\ pulses\ recorded}{number\ of\ radiation\ quanta\ emitted\ by\ source} \tag{5.2}$$

Differently from total efficiency, where all interactions, no matter how low in energy, are accepted, *peak efficiency* assumes that only those interactions that deposit the full energy of the incident radiation are counted, and the number of full energy events can be obtained by simply integrating the total area under the peak. It is often preferable from an experimental standpoint to use only peak efficiencies, because the number of full energy events is not sensitive to some perturbing effects, such as scattering from surrounding objects or spurious noise.
Figure 5.3 shows an example of spectrum obtained with the ^{152}Eu source and using a cylindrical scintillator.

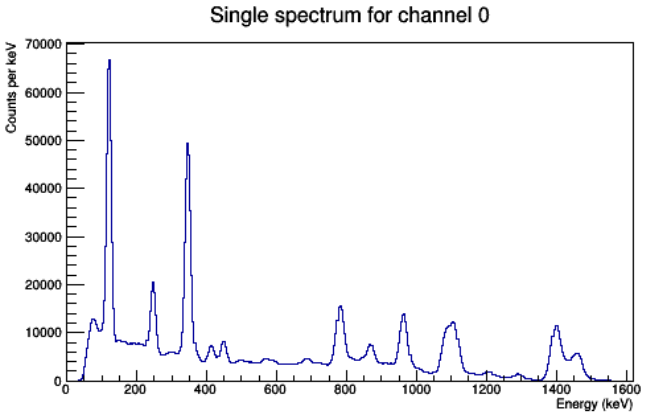

Figure 5.3: Energy spectrum of ^{152}Eu source obtained from a single cylindrical scintillator with a PM voltage of 1200V.

For each group of scintillators we calculate the total number of pulses recorded at a specific energy by integrating the total area, with the background subtracted, under every chosen peak of each single channel ($A_{ch_j}(E_\gamma)$) and then we sum them together, keeping separated the calculation for the two kind of detectors.

The number of radiation quanta, emitted by source at a certain energy, instead, is given by the product of activity of the source, time of measure (t) and intensity of the gamma (I_γ) so 5.2 becomes:

$$\epsilon_{abs}(E_\gamma) = \frac{\sum_{j=1}^{channel\ N} A_{ch_j}(E_\gamma)}{Activity\ t\ I_\gamma} \tag{5.3}$$

where the activity of the source at time data were recorded has been calculated from the known activity as measured at known time, reported in table 4.1, and applying the radiation-decay law which asserts that the activity of a source decreases in time as $A(t) = A_0 e^{\lambda t}$ where λ is the decay constant of ^{152}Eu which can be calculate knowing that the half-life of the decay is about 13.5 years. The time of

measure was two hours and a half, so it was approximated that the activity was constant during this time, and gamma-ray intensities for the nine peak selected have been obtained by tables in Ref. [9] . All these informations are reported in table 5.2 and 5.3.

Table 5.2: Activity of ^{152}Eu source at time measurement and time of measure.

Activity (kBq)	time (s)
254 ± 2	9000 ± 2

Table 5.3: Gamma-ray Energies and Absolute Intensities

E_γ(keV)	121.7817±0.0003	244.6975±0.0008	344.2785±0.0013	411.1165±0.0013	444.0
I_γ(%)	28.37±0.13	7.53±0.04	26.57±0.13	2.238±0.010	3.125±0.014

E_γ(keV)	778.9045±0.0024	867.378±0.004	964.1	1408.011±0.004
I_γ(%)	12.97±0.06	4.214±0.025	14.63±0.06	20.85±0.09

Using equation 5.3 the efficiency of the two kind of $LaBr_3$(Ce) array could be calculated at various energies. Figure 5.4 shows the values obtained. We notice then in both cases the efficiency decrease with energy but this reduction is faster for detector of smaller size, the truncated cone ones (red points). The size and shape of the scintillation crystal have a strong influence on the counting efficiency. Although the major influence on the intrinsic efficiency is the thickness of the crystal in the direction of the incident gamma radiation, mild variation with other detector dimension should also be expected. The size and physical nature of the source can also influence the counting efficiency together with the source-detector spacing, the more the source is near the detectors the more the probability of detect the gamma ray increases.

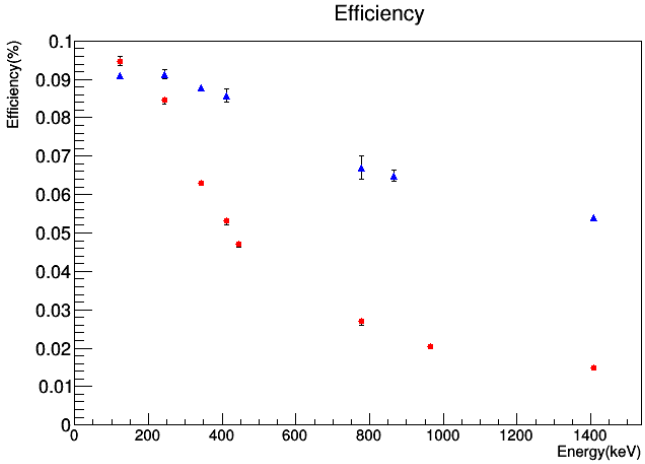

Figure 5.4: Absolute photopeak efficiencies for the truncated cone (red points) and cylindrical (blue point) detector measured with an calibrated ^{152}Eu source placed at 10 cm from the detectors.

A function used to describe the relationship between efficiency and energy is given by equation 5.4.

$$\epsilon_{abs}(x) = e^{p(x)} \quad p(x) = A_0 + A_1 ln(x) + A_2 (ln(x))^2 + A_3 (ln(x))^3 + ... \tag{5.4}$$

$$x = \frac{E_\gamma(keV)}{100}$$

The expansion of p(x) can be truncated at the third order with good approximation and A_0, A_1,A_2,

A_3 are parameters to be fit. Figure 5.5 shows the linearized 5.4 equation with the fit curves and table 5.4 reports the fit parameters calculated.

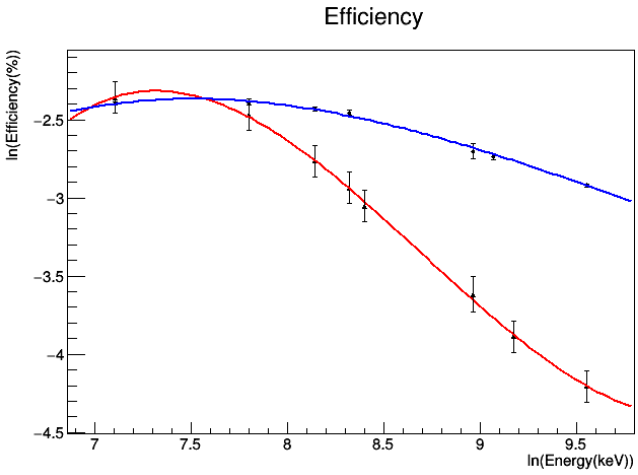

Figure 5.5: Linearized efficiency and fits with equation 5.4 for the two kind of detectors, the truncated cone (red line) and cylindrical (blue line).

Table 5.4: Fit parameters

Geometry	A0	A1	A2	A3	$\frac{\chi^2}{ndf}$
Cylinder	-23.66 ±0.04	7.12±0.01	-0.763±0.001	0.0257±0.0001	2.67/3
Truncated cone	-124.3±0.3	43.97±0.06	-5.184±0.006	0.1987±0.0005	0.24/4

5.1.3 Timing performance

The definition and the description of the main characteristics of a time spectrum obtainable with a scintillator detector have been discussed in section 3.3. For the measure of timing resolution attainable for a pair of truncated cone $LaBr_3(Ce)$ detectors we collected data from a radioactive source of a ^{60}Co at 1100V, testing various combination of CFD parameters in order to obtain the best resolution. We also made a measurement with a couple of cylindrical scintillator to have a term of comparison, but we focussed our attention on the smaller size detectors because of their greater time resolution, suitable for the measure of ^{152}Sm. Timing data were sorted into a three-dimensional (energy, energy, time) histogram, processed off-line and analyzed with ROOT. The analysis comprises the selection of the energy gates and the sorting of the final time spectra with the chosen energy condition.

The time difference is simply measured in one direction as :

$$dt_{21} = t_2 - t_1 \tag{5.5}$$

Here, the detector 2 represents the stop signal and the start signal is given by detector 1. Selecting a gamma ray which directly feeds a nuclear state with the start detector 1, in our case the 1173-keV transition, ad the decay gamma ray, the 1333-keV transition, with the stop detector 2, the time distribution is obtained by time projecting the 3D histogram.

Figure 5.6 (a), (b) and (c) show, respectively, an example of the 3D (energy, energy, time) cube, his projection on the (energy, energy) plane which highlights the $\gamma-\gamma$ coincidence and the time projection with an energy selection.

We made a comparison between time spectra obtained in one direction (dt_{21}) both with and without gates in energy and time spectrum obtained with a couple of cylindrical detectors. The results of a

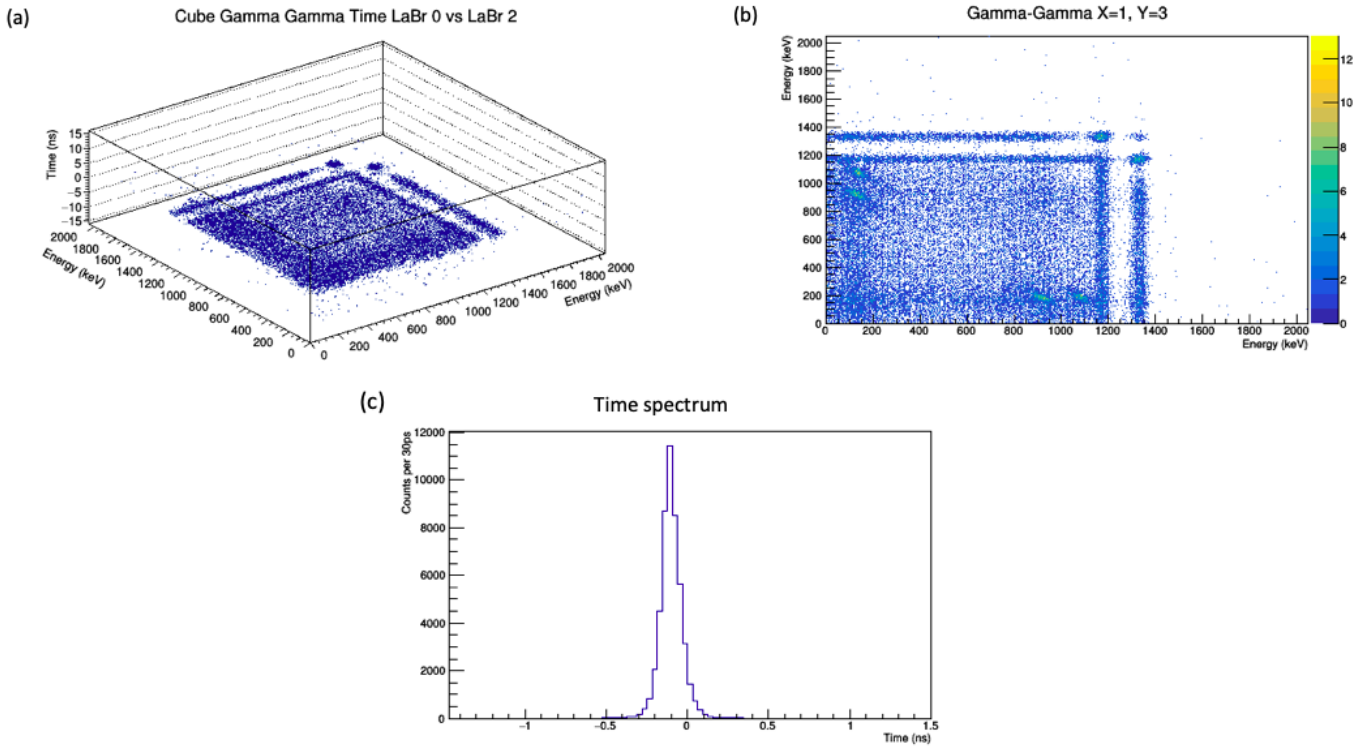

Figure 5.6: (a) Example of an (energy, energy, time) histogram taken at 1100V with a couple truncated cone scintillator and a source of ^{60}Co $LaBr_3$(Ce). (b) Projecton of the 3D cube on the (energy, energy) plane. (c) Time spectrum corresponding to the 2^+ state in ^{60}Ni from a detector pair, obtained by collecting data started by 1173-keV γ ray from the decay of a ^{60}Co and stopped by the 1337-keV ray.

measurement at 1100V with a CFD fraction of 50%, a delay of 1 ns and a CFD interpolation of 1, are reported in table 5.5. They show that the energy resolution of the truncated cone detectors is greatly better than the cylindrical one, this is mainly due to the smaller size, infect when a γ ray emitted by the source enters in the active volume of the scintillator it products light that spreads out in all directions, if the detector is big, this light takes a longer time to get the PMT tube and arrives in less quantity respect to a smaller detector. This entails that the rise-time of the pulse signal produced is slower and the precise determination of the t start by the CFD becomes more complicated. Also the use of energy gates improves substantially the time resolution, and for this reason it is important to have detectors with a good energy resolution.

Table 5.5: Comparison between FWHM of the time spectra measured at 1100V with the same CFD configuration.

Configuration	Cilindrical with gate	Truncated cone no gate	Truncated cone with gate
FWHM (ns)	1.95±0.01	0.509±0.005	0.29±0.02

In each measure with different CFD parameters we have also recorded the time difference in the other time direction $dt_{12} = t_1 - t_2$ by inverting the energy selection in the detectors, we calculated the centroids of the two sorted time spectra and aligned them together. Finally we superimpose the data, obtaining a mirror-symmetric total time spectrum. Figures 5.7 (a) and (b) show an example of this procedure [7].

This spectrum has the appearance of a Gaussian because it is a convolution of a prompt time distribution and the exponential nuclear-decay distribution in the limit of a small lifetime. The final coincidence resolution time for the ^{60}Co source is given as the FWHM of the summed time peak. Table 5.6 shows the time resolutions obtained with the combination of CFD parameters tested.

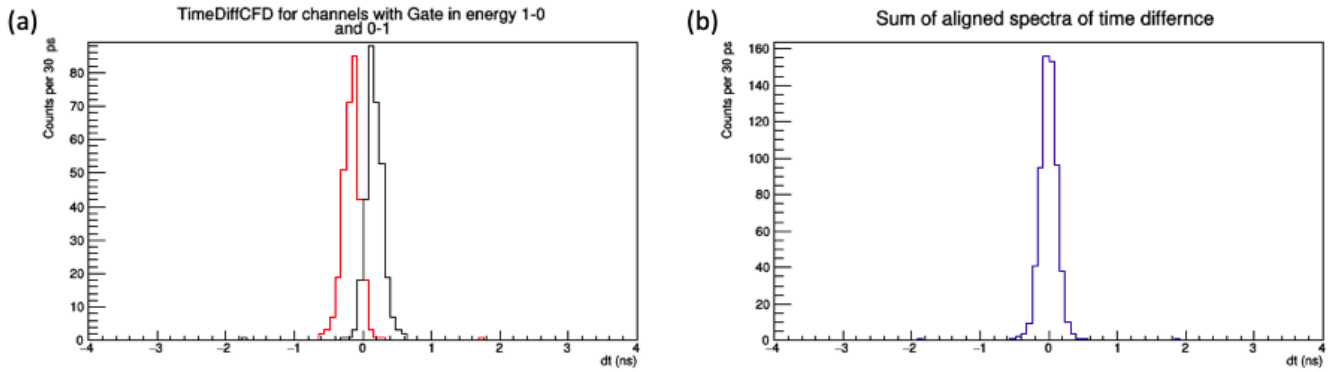

Figure 5.7: (a) Two independent time distributions obtained with a source of ^{60}Co and energy gates set at the 1173-keV full-energy peak in detector 1 and 1332-kev full-energy peak in detector 2 and vice versa. (b) Sum of the two time spectra in figure (a) after synchronization to 0 ns.

Table 5.6: CFD parameters and Time resolution measured at 1100V with a ^{60}Co source

CFD fraction	CFD Interpol	CFD Delay (ns)	Time resolution (ns)
25 %	1	3	0.283±0.09
50 %	1	3	0.30±0.01
50 %	1	6	0.32±0.09
50 %	1	2	0.27±0.09
50 %	1	1	0.32±0.09

Since the combination of CFD fraction 50%, CFD interpolation 1 and CFD delay 2 ns provides the best time resolution we use this configuration for the measure of a ^{152}Sm state lifetime. In our case, the dominant error contribution in the evaluation of the time resolution is the jitter, as will be shown in the next section.

5.2 Measure of ^{152}Sm lifetime

For the lifetime measure of the 121-keV energy state of ^{152}Sm, coming from the β decay of ^{152}Eu, a couple of truncated cone scintillators was used and the parameters of the CFD inside the digitizer were set at the values found in the previous section. A long measure of two days has been performed. Energy gates were set at the 121-keV full energy peak on the first detector and at coincidence 1408-keV full energy peak on the other detector, and vice versa.

Since the lifetime of this state is longer than the statistical time resolving power of the set-up, as previously mentioned, the experimentally obtained delayed time distribution corresponds to a convolution of the energy-dependent prompt time distribution P(t) with an exponential decay as :

$$D(t) = n\lambda \int_{t_-}^{t} P(t_0 - t')\, e^{\lambda(t-t')}\, dt' \quad with \quad \lambda = \frac{1}{\tau} \tag{5.6}$$

where n is the number of counts in the time distribution, t_0 is the centroid of P(t) and t_- indicates the lower integration limit where P(t_-)=0. λ and τ are the transition probability and the mean lifetime of the excited state [7].

By fitting the exponential tail of the distribution, the decay constant, together with the lifetime of the intermediate state, can be simply deduced. Figure 5.8 shows one of the two symmetric time spectra obtained and in Table 5.7 the results of the fit and the lifetime values are reported.

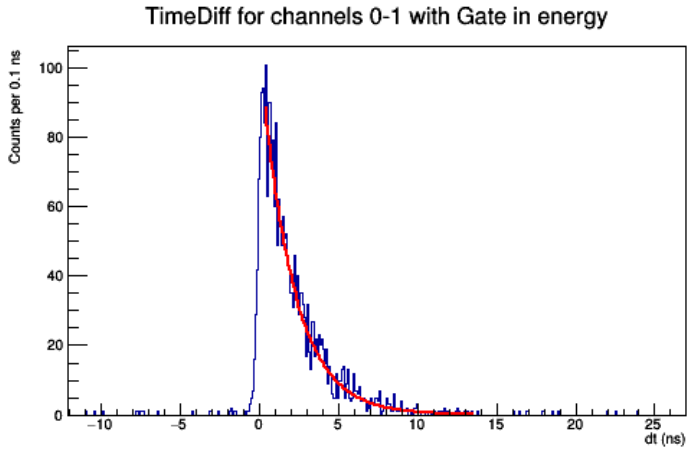

Figure 5.8: Time spectrum corresponding to the 2^+ state in ^{152}Sm, obtained from a pair of detectors by collecting data started by 1408-keV γ ray from the decay of a ^{152}Eu source and stopped by the 121-keV ray.

Table 5.7: Decay constants λ obtained by the exponential fit on the two time spectra with inverted channel selection and the lifetime τ values calculated as $\lambda = \frac{1}{\tau}$.

Channels	λ (ns^{-1})	τ (ns)	$\frac{\chi^2}{ndf}$
0-1	0.496±0.012	2.02±0.05	121.9/110
1-0	0.499±0.011	2.00±0.05	101.2/101

The average value of the lifetime and literature value obtained from ref. [8] are in very good agreement, as it is shown in the Table 5.8, which also summarizes all the characteristics of the analyzed nuclear state:

Table 5.8: Experimental result τ of lifetime measurement using a a pair of $LaBr_3$(Ce) scintillator detectors.

Nucleus, state (keV)	Spin J^π	γ_{feeder}-γ_{decay} cascade (keV)	τ_{lit} (ns)	τ(ns)
^{152}Sm, 121	2^+	1408-121	2.010±0.033	2.02±0.02

With the same collected data, we have also estimated the time jitter and the time walk (see Chapter 3) of the $LaBr_3$(Ce) scintillators pair, by taking advantage of the offline analysis and the possibility of changing the energy gates selection. γ rays of various energies, in coincidence with the 244-keV internal transition γ ray in ^{152}Sm, were used as the start signal and the 244-keV γ ray was used as the stop signal, and vice versa. This specific γ ray was chosen because it presents a large range of possible transition energies in coincidence, whose decay populate the 4^+ state. The resultant spectra show the typical exponential-Gaussian convolution form.

The σ parameters of the time spectra for each energy were taken to be the time jitter and they are reported in Figure 5.9 and fitted with a function similar to equation 5.11, defined for the time walk. In Table 5.9 the parameters of this function are shown. The time jitter includes all possible experimental deviation from the ideal time pick-off of instantaneously occurring prompt gamma-gamma events, represented by a δ function. As already mentioned, the time measurements are the resultant of a subtraction of start time from stop time. Thus error propagation suggests that the observed uncertainty is the quadrature sum of the errors of the two component measured, assuming that jitter is the dominant source of statistical error and that the measurements are independent.

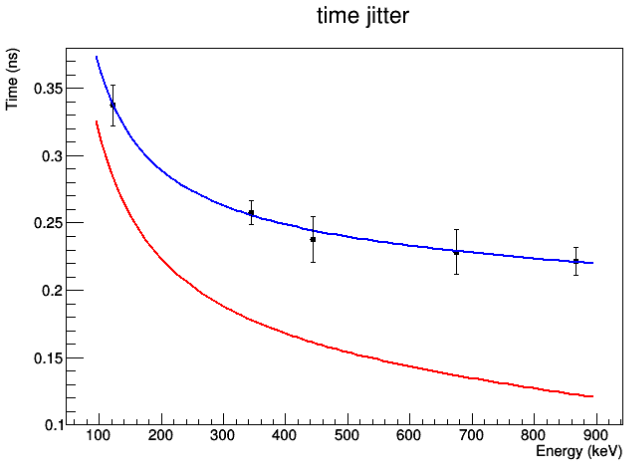

Figure 5.9: Time jitter measured as a function of energy (blue line). The lower line (red) indicates the component contribution of the start event and stop event (see text for more details).

Parameter	value
a ($ns\,keV^{\frac{1}{2}}$)	1±2
b (keV)	0.1±0.1
c ($ns\,keV^{-1}$)	0.00002±0.00003
d (ns)	0.22±0.03

Table 5.9: Parameter values describing the time jitter, resulting from the fit of the data with function 5.11.

If σ_t(E) is the observed uncertainty at energy E, then it holds that:

$$\sigma_t(E)^2 = \sigma'_t(E)^2 + \sigma'_t(244(keV))^2 \tag{5.7}$$

where $\sigma'_t(E)$ is the component error due to a single start or stop event. By evaluating this equation for E=244 we obtain that $\sigma_t(244)^2 = 2\sigma'_t(244)^2$ and rearranging to solve for $\sigma'_t(E)^2$:

$$\sigma'_t(E) = \sqrt{\sigma_t(E)^2 - \frac{1}{2}\sigma_t(244)^2} \tag{5.8}$$

Equation 5.8 was used to produce the line below the data points in figure 5.9. Generalizing Equation 5.7 to an arbitrary energy pair, the following equation is obtained:

$$\sigma_t(E_1, E_2) = \sqrt{\sigma'_t(E_1)^2 + \sigma'_t(E_2)^2} \tag{5.9}$$

where $\sigma_t(E_1, E_2)$ is the observable resolution from a timing measurements with start and stop energies corresponding to E_1 and E_2. As $\sigma'_t(E)$ is plotted on figure 5.9 (lower line), a visual solution of the last equation is to simply sum, in quadrature, the jitter value at the two energies. Evaluating this equation for the ^{60}Co energies, the jitter found is about 135 ps which is compatible with the σ values of the time distributions analyzed in the previous section for the time resolution, and this confirms that the jitter is the dominant source of statistical error.

The time at which the CFD signal output is generated depend on the characteristics of the input signal, such for example the charge sensitivity, the input signal amplitude and input signal noise. The systematic timing uncertainty due to the dependence of the prompt response function PRF centroid to the γ energies is called the time-walk of the signal. As described by *Régis et al.* [7], the time walk can be corrected by constructing a prompt response difference function (PRDF) using γ ray timing data from a ^{152}Eu source. The PRDF can be described by equation:

$$PRDF(E) = \frac{a}{\sqrt{E+b}} + cE + d \tag{5.10}$$

where E is the energy of the photon measured, and a, b, c and d are free parameters. Using the same time spectra constructed for the evaluation of time jitter we obtained the centroids of the two

symmetric time distribution, with reversed energy gating conditions. Each of the γ ray pair was used to create prompt response function by taking the centroid difference. Figure 5.10 (a) shows the centroids distribution in function of the energy, instead Figure 5.10 (b) displays the prompt response difference function with the fit resultant from a least-squares minimization procedure.

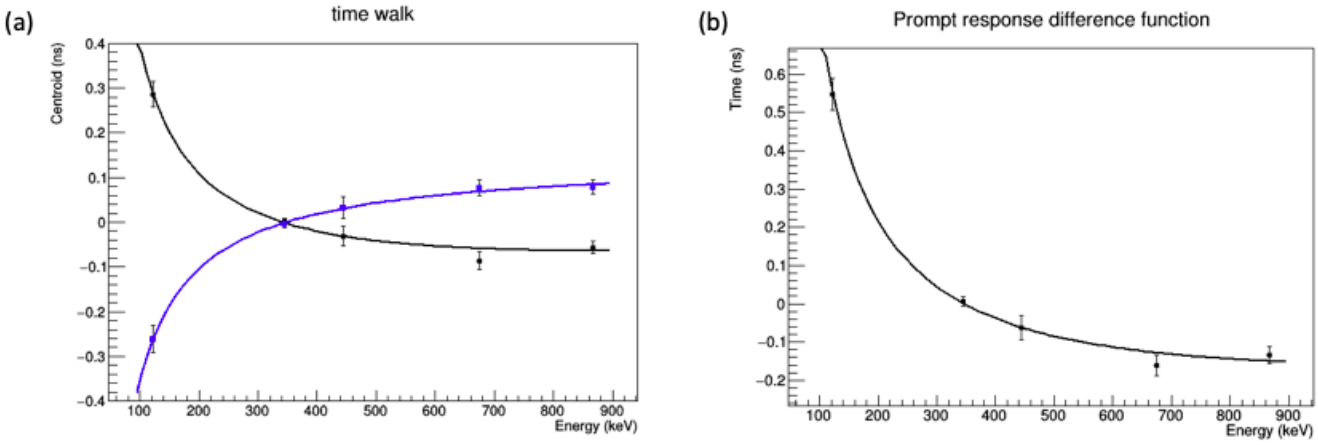

Figure 5.10: (a) Centroid shift analyzes on the time walk for a couple of truncated cone scintillators. (b) The PRDF curve obtained from centroid difference measurements. The solid line is the result of a least-square minimization procedure to describe the data points.

The parameters of equation 5.11 get from the fit are reported in Table 5.10.

Table 5.10: Parameter values describing the prompt response function, resulting from the fit to the data.

Parameter	value
a ($ns\,keV^{\frac{1}{2}}$)	7±24
b (keV)	0.07±0.23
c ($ns\,keV^{-1}$)	0.000068±0.000066
d (ns)	-0.332±0.055

The prompt response difference between two γ ray energies can be calculated as $PRD(E_1, E_2) = PRDF(E_1) - PRDF(E_2)$ where E_1 and E_2 are the energies of the feeding and decaying transition rays of the state to be measured, respectively. The PRD permits the correction of the lifetime measurement since it is connected to the centroid difference by equation:

$$\Delta C(E_1, E_2) = PRD(E_1, E_2) + 2\tau \tag{5.11}$$

This kind of correction is really relevant in lifetime measurement based on the generalized centroid-difference method [10], typically used for the sub-nanosecond region. For example, at ^{60}Co energies the values of PRD obtained with this kind of calculation is about 3 ps and considering that the lifetime value of the 1333 keV-energy state is about 1.11 ps [8], it can not be neglected. However, with lifetime in the nanosecond region measured with the slope method, like in our experiment, this correction does not affect our final lifetime value since it will caused only a rigid translation of the whole spectrum.

Chapter 6

Conclusion and perspectives

In this work, after discussing the main characteristics and components of a scintillator detector, together with the main pick-off methods in timing measurements, energy resolution, efficiency and timing performance of 7 $LaBr_3$(Ce) scintillators, with two different geometries, have been evaluated. Three detectors presents a 3"x3" cylindrical crystal coupled to an Hamamatsu R9779 photomultiplier tube and four detectors a 1.5"x1.5"x1" truncated cone crystal coupled to an Hamamatsu R6233-100SEL PMT. Both energy and time informations were processed digitally inside a CAEN V1730B digitizer.

The FWHM energy resolution measured at ^{137}Cs energies and at 1200V was 31.83±0.05 keV (4.8%) and 30.84±0.05 keV (4.7%) for the cylindrical and truncate cone crystal respectively, and similar values were obtained also at 1100V, reveling that the voltage does not affect in a relevant way this particular quantity. Also the geometry seems not influence energy resolution, except for low energy as fig 5.2 reveals.

The absolute photopeak efficiency was instead evaluated at various energies using a ^{152}Eu source and values in the range 0.02%-0.1% were obtained (fig.5.4). For both geometry efficiency decrease with energy but this reduction is faster for detector of smaller size, the truncated cone ones. As a matter of fact, the size and shape of the scintillation crystal have a strong impact on the counting efficiency.

The detector time response has been optimized by the tuning of the electronics parameters. Testing different combinations of the constant fraction discriminator parameters we tried to obtained the best resolution value possible in our experimental conditions. This time resolution, evaluated at ^{60}Co energies as the FWHM of the time spectrum for individual truncated cone detector was 0.27±0.09 ns, and 1.95±0.01 ns for the cylindrical scintillators. Therefore, the truncated cone $LaBr_3$(Ce) crystal presents the best time response and it is vert well suited for fast-timing applications.

Finally, the lifetime τ of the 121keV-energy state of ^{152}Sm has been measured thanks to the slope method, the best choice for nanosecond region. In this case, the experimentally "delayed" time distribution is a convolution of the normalized prompt response function with an exponential decay and the lifetime is obtain by a simple fit of the exponential tail of the distribution. The value obtained was τ= 2.02 ±0.02 ns. Time jitter and walk were also characterized, and the jitter turns out to be the dominant error contribution in the time resolution, while the time-walk effects do not influence our measurement but could become relevant for picosecond-sensitive time-difference measurements.

In this work, for the first time, fast-timing measurements were done all in digital, without the traditional analog chain. Scintillator detectors output was directly connected to the digitizer input, where all the manipulations on the signal pulses are done. This will open new opportunities and with better digitizers we can achieve the same time resolution than analog systems or even better.

Bibliography

[1] G. F. Knoll, *Radiation Detection and Measurements*, 4^{th} Edition, Jogn Wiley & Sons Inc., 2010.

[2] A. Giaz et al., *Characterization of large volume 3.5"x8" $LaBr_3$(Ce) detectors*, Nucl. Instrum. Methods Phys. Res. A 729(2013) 910-921.

[3] V. Vedia et al., *Performance evaluation of novel $LaBr_3$(Ce) scintillator geometries for fast-timing applications*, Nucl. Instrum. Methods Phys. Res. A 857(2017) 98-105.

[4] https://www.caen.it/products/v1730.

[5] https://www.sparrowcorp.com/products/software.

[6] User Manual WP2081, Digital Pulse Processing in Nuclear Physics, Overview of CAEN DPP algorithms, Rev.4 (2017).

[7] J.-M. Régis et al., *A simple procedure for. γ- γ lifetime measurements using multi-element fast-timing arrays*, Nucl. Instrum. Methods Phys. Res. A 897(2018) 38-46.

[8] National Nuclear Data Center http://www.nndc.bnl.gov.

[9] *X-ray and Gamma-ray Standards for Detector Calibration*, report by the Co-ordinated Research IAEA Programme, IAEA-TECDOC-619 (1991)

[10] J.-M. Régis et al., *The generalized centroid difference method for picosecond sensitive determination of lifetimes of nuclear excited states using large fast-timing arrays*, Nucl. Instrum. Methods Phys. Res. A 729(2013) 191-202.